NeuroImage 54 (2011) 963–973

Contents lists available at ScienceDirect

NeuroImage

journal homepage: www.elsevier.com/locate/ynimg

Lesion Explorer: A comprehensive segmentation and parcellation package to obtain regional volumetrics for subcortical hyperintensities and intracranial tissue

J. Ramirez [a,b,c,e,*], E. Gibson [a,b,c], A. Quddus [a,c], N.J. Lobaugh [a,b,c], A. Feinstein [c,d,e], B. Levine [f], C.J.M. Scott [a,b,c], N. Levy-Cooperman [a,b,c,e], F.Q. Gao [a,b,c], S.E. Black [a,b,c,e,f]

[a] LC Campbell Cognitive Neurology Research Unit, Canada
[b] Heart & Stroke Foundation Centre for Stroke Recovery, Canada
[c] Sunnybrook Health Sciences Centre, Brain Sciences Research Program, Sunnybrook Research Institute, Canada
[d] Sunnybrook Multiple Sclerosis Research Unit, Canada
[e] University of Toronto, Institute of Medical Science, Faculty of Medicine, Canada
[f] Rotman Research Institute, Baycrest, Canada

ARTICLE INFO

Article history:
Received 17 March 2010
Revised 1 September 2010
Accepted 3 September 2010
Available online 19 September 2010

Keywords:
MRI
Aging
Alzheimer's disease
White matter hyperintensities
Leukoariosis
Segmentation
Lesion analysis
Brain volume

ABSTRACT

Subcortical hyperintensities (SH) are a commonly observed phenomenon on MRI of the aging brain (Kertesz et al., 1988). Conflicting behavioral, cognitive and pathological associations reported in the literature underline the need to develop an intracranial volumetric analysis technique to elucidate pathophysiological origins of SH in Alzheimer's disease (AD), vascular cognitive impairment (VCI) and normal aging (De Leeuw et al., 2001; Mayer and Kier, 1991; Pantoni and Garcia, 1997; Sachdev et al., 2008). The challenge is to develop processing tools that effectively and reliably quantify subcortical small vessel disease in the context of brain tissue compartments. Segmentation and brain region parcellation should account for SH subtypes which are often classified as: periventricular (pvSH) and deep white (dwSH), incidental white matter disease or lacunar infarcts and Virchow–Robin spaces. Lesion Explorer (LE) was developed as the final component of a comprehensive volumetric segmentation and parcellation image processing stream built upon previously published methods (Dade et al., 2004; Kovacevic et al., 2002). Inter-rater and inter-method reliability was accomplished both globally and regionally. Volumetric analysis showed high inter-rater reliability both globally (ICC = .99) and regionally (ICC = .98). Pixel-wise spatial congruence was also high (SI = .97). Whole brain pvSH volumes yielded high inter-rater reliability (ICC = .99). Volumetric analysis against an alternative kNN segmentation revealed high inter-method reliability (ICC = .97). Comparison with visual rating scales showed high significant correlations (ARWMC: r = .86; CHIPS: r = .87). The pipeline yields a comprehensive and reliable individualized volumetric profile for subcortical vasculopathy that includes regionalized (26 brain regions) measures for: GM, WM, sCSF, vCSF, lacunar and non-lacunar pvSH and dwSH.

Introduction

Subcortical hyperintensities (SH) are frequently observed on T2-weighted MRI of the aging brain (Jack et al., 2001; Kertesz et al., 1988; Longstreth et al., 1996). Clinico-pathological correlations suggest vascular and degenerative origins including: ischemic tissue damage via arteriosclerosis (Babikian and Ropper, 1987; van Swieten et al., 1991); vasogenic edema from periventricular venous collagenosis (Black et al., 2009; Gao et al., 2008; Moody et al., 1995); multiple lacunar infarcts (Longstreth et al., 1996); état criblé or dilated perivascular spaces (Awad et al., 1986); demyelination and sub-ependymal gliosis; amyloid angiopathy (Pantoni and Garcia, 1997); and clasmatodendrosis (Sahlas et al., 2002).

Although the pathophysiological origins are not fully understood, the current literature suggests that SH: are common after age 60 (Longstreth et al., 1996); share common cerebrovascular risk factors such as diabetes and hypertension (De Leeuw et al., 2001; Liao et al., 1996; Sachdev et al., 2008); and are associated with increased risk of cognitive decline, stroke, gait disorders and neuropsychiatric disorders (De Groot et al., 2001; Koga et al., 2009; Longstreth et al., 1996, 2005; Srikanth et al., 2009; Vermeer et al., 2003a,b). To further assess the effects of vascular risk factors in overt and covert cerebrovascular disease and in dementia, consensus criteria were developed that underline the importance of accounting for SH in studies on aging (Hachinski et al., 2006).

Although visual scales can provide quick ratings of SH severity on MRI (Bocti et al., 2005; Fazekas et al., 1987; Scheltens et al., 1993; Wahlund et al., 2001), inconsistencies in methodological properties

* Corresponding author. LC Campbell Cognitive Neurology Research Unit, Sunnybrook Health Sciences Centre, A421-2075 Bayview Avenue, Toronto, Ontario, Canada, M4N 3M5.
E-mail address: joelr@sri.utoronto.ca (J. Ramirez).

1053-8119/$ – see front matter © 2010 Elsevier Inc. All rights reserved.
doi:10.1016/j.neuroimage.2010.09.013

(Mantyla et al., 1997) have led some researchers to apply intensity-based segmentation techniques that provide a more accurate estimation of SH burden — as well as quantify their extent and location. However, typical T1-based tissue segmentation techniques that do not explicitly segment T2 hyperintensities can inflate other tissue volumes. Depending on the segmentation technique used, gray matter volumes can be overestimated by failing to segment the hyperintensities (Levy-Cooperman et al., 2008), see Fig. 7 for example.

Quantitative segmentation approaches have been applied to capture SH on T2, proton density (PD) and fluid-attenuated inversion recovery (FLAIR) images. Some of the recent approaches in the last decade include: fuzzy clustering models that include a lesion class (Admiraal-Behloul et al., 2005; Gosche et al., 1999); Gaussian curve fitting to determine lesion intensity cut-off points (Decarli et al., 2005a); modal intensity cut-offs applied to slice-by-slice intensity histograms (Jack et al., 2001); k-Nearest Neighbor (kNN) algorithmic combination approaches (Anbeek et al., 2004; Seghier et al., 2008; Swartz et al., 2002; Wen et al., 2008); and coregistration to normal templates comparing the voxel-wise SH probabilities from FLAIR images to a white matter probability map using a weighting function (Burton et al., 2004; Wen and Sachdev, 2004). These approaches range from fully automated to semi-automated labor intensive processes.

Fully automated techniques offer the advantage of high reliability and are preferable for processing large scale studies. They typically require FLAIR imaging, where SH are often more conspicuous relative to standard PD/T2 images. However, FLAIR imaging is less sensitive in detecting focal thalamic lesions (Bastos Leite et al., 2004; Jack et al., 2001) and was not included in the multi-center Alzheimer's Disease Neuroimaging Initiative (ADNI) acquisitions (Jack et al., 2008). Furthermore, FLAIR imaging alone cannot disambiguate the possible heterogeneity that is implicated in SH pathology.

In an attempt to address the hypothesis of pathological heterogeneity within SH, various subtypes have been suggested for further segmentation. One common, albeit controversial, distinction is between periventricular (pvSH) and deep white (dwSH) subcortical hyperintensities (Decarli et al., 2005a; Sachdev and Wen, 2005). Although dwSH and pvSH volumes are correlated (Decarli et al., 2005a), some studies have shown pvSH and dwSH to be differentially associated with: gray matter atrophy; ventricular dilatation; and cognitive, behavioral and motor/gait performance (Sachdev and Wen, 2005; Sachdev et al., 2005; Silbert et al., 2008).

Lack of a standardized methodology for the definition of pvSH may be the cause of inconsistent reports in the literature. The typical method to distinguish pvSH from dwSH is to create an arbitrary two-dimensional cut-off line lateral to the ventricles on axial slices in a slice-by-slice manner. This arbitrary line is sometimes calculated as a proportional distance from the ventricular border to the dura mater (Decarli et al., 2005a), or set using an arbitrary voxel distance from the ventricle out into the centrum semiovale. Some reviewers have suggested that there may be some neuroanatomic justification for classifying SH within a 13 mm rim around the ventricle as pvSH (Mayer and Kier, 1991; Sachdev et al., 2008). Various other methods arbitrarily delineate pvSH from dwSH using a linear distance calculation. However, a standardized, unbiased method that recognizes the 3-dimensional nature of SH would be preferable.

Other subtypes of SH include perivascular (Virchow–Robin) spaces and cystic fluid-filled lacunar-like infarcts. Virchow–Robin (VR) spaces are CSF-filled extensions of the subarachnoid space in the sheath surrounding blood vessels. They appear as hyperintense dots or lines on T2 images, are isointense on PD and typically 1 mm or less in diameter (Awad et al., 1986). Their size, shape, and differential appearance on T2 and PD allow them to be distinguished from other SH subtypes — including lacunes.

Automatic segmentation of lacunes is less common since this requires coregistration of T2/PD/FLAIR images to a T1-based segmentation, in order to identify CSF intensity within SH. Lacunes are associated with aging, hypertension, increased risk of stroke, and are found in 11–28% of elderly (Longstreth et al., 1998; Vermeer et al., 2003b, 2007). These so-called silent strokes or covert infarcts, are usually defined as 3–15 mm in diameter, are hypointense on T1, and hyperintense on both T2 and PD images. Their presence is associated with increased risk of dementia and have been correlated with decreased frontal lobe glucose metabolism with positron emission tomography (PET) imaging (Reed et al., 2004). However, without a coregistered T1-segmentation and PD-T2 contrast for comparison, lacunes and VR spaces are difficult to quantify through volumetric segmentation with FLAIR alone.

An additional benefit of a T1-based tissue segmentation combined with PD-T2-based SH segmentation is that it allows for relative volumetric tissue comparisons for gray matter (GM), white matter (WM), ventricular-CSF (vCSF) and sulcal-CSF (sCSF). However, whole brain global volumetrics alone provide limited information, and regionalized quantification, whether ROI-based or template-based, has become a standard expectation for any MRI-based segmentation procedure.

Hence, the need for a comprehensive, individualized MRI processing pipeline that reliably segments the brain into regionalized tissue compartments and includes the various SH subtypes has become increasingly important. Lesion Explorer (LE) is the final component of an MRI-based processing pipeline that was developed with these considerations. It was built upon updated versions of two previously published components: an automated T1-based tissue segmentation protocol (Kovacevic et al., 2002); and the Semi-Automated Brain Region Extraction (SABRE) parcellation procedure (Dade et al., 2004). The LE pipeline makes use of 3 processing components that effectively allow comprehensive analysis of individual brains through the segmentation of 8 tissue classes: GM, WM, sCSF, vCSF, lacunar and non-lacunar pvSH and dwSH — tissue volumes are then parcellated into 26 SABRE brain regions. Inter-rater and inter-method reliability data is presented with validation against an alternative kNN segmentation approach and 2 different visual rating scales.

Materials and methods

Subjects

Images used for this study (n = 20) were selected from participants in the Sunnybrook Dementia Study — a large ongoing longitudinal observational study conducted in the LC Campbell Cognitive Neurology Research Unit and the Heart & Stroke Foundation Centre for Stroke Recovery (http://www.heartandstroke-centrestrokerecovery.ca) at Sunnybrook Health Sciences Centre, a University of Toronto academic healthcare institution. See Table 1 for additional details. Exclusion criteria for this sub-study included: Parkinson's disease or other neurological diseases other than dementia, history of significant head trauma, psychotic disorders unrelated to dementia, psychoactive substance abuse and major depression. Participants in this study had a historical profile typical of AD with insidious onset of short term memory loss. All patients received a standardized comprehensive clinical evaluation. The presence of cerebrovascular risk factors was ascertained including: arterial hypertension, diabetes, hyperlipidemia, and cardiac disorders such as coronary artery disease. All patients in this study met National Institute of Neurological and Communicative Disorders and Stroke–Alzheimer's Disease and Related Disorders Association criteria for probable or possible AD, (McKhann et al., 1984) and Diagnostic and Statistical Manual of Mental Disorders — Fourth Edition (American Psychiatric Association, 1994) criteria for dementia.

MRI acquisition

All brain imaging data was obtained on a 1.5 T GE Signa (Milwakee, WI) system in compliance with the consensus panel imaging

Table 1
Demographics and whole brain raw volume lesion data.

Ss	Reviewed Dx	Sex	YOE	Age	Rater 1 SH volume (mm^3)	Rater 2 SH volume (mm^3)	Absolute volume difference
1	AD	M	11	75	2043	2291	248
2	AD + VaD	M	15	78	40,961	40,971	10
3	AD + VaD	M	16	77	68,456	68,648	192
4	AD	M	19	71	4697	4789	92
5	AD + VaD	M	17	73	49,267	49,917	650
6	AD + VaD	F	12	88	20,696	20,904	208
7	AD	F	12	68	4777	4616	161
8	AD + CVD	F	8	87	10,152	10,528	376
9	AD + CVD	F	13	84	12,053	11,938	115
10	AD + VaD	F	14	73	19,900	19,698	202
11	AD + CVD	F	17	74	13,986	14,372	386
12	AD + VaD	F	10	78	26,317	26,348	31
13	AD	M	20	76	8059	8121	62
14	AD + CVD	F	19	72	16,920	16,926	6
15	AD	F	14	83	2077	2426	349
16	AD + CVD	F	17	64	4844	4816	28
17	AD	F	12	68	5529	5621	92
18	AD + CVD	M	18	76	3710	4318	608
19	AD	F	17	79	8981	8382	599
20	AD	M	23	66	3725	3927	202
						Mean	230.85

recommendations on VCI (Hachinski et al., 2006). Three image sets were used: a T1-weighted (axial 3D SPGR: 5 ms TE, 35 ms TR, 1 NEX, 35° flip angle, 22 × 16.5 cm FOV, 0.859 × 0.859 mm in-plane resolution, 1.2 to 1.4 mm slice thickness depending on head size), with an interleaved PD and T2 (interleaved axial dual-echo spin echo: TEs of 30 and 80 ms, 3 s TR, 0.5 NEX, 20 × 20 cm FOV, 0.781 × 0.781 mm in-plane resolution, 3 mm slice thickness).

Age-Related White Matter Changes (ARWMC)

A previously published consensus-derived rating scale developed under the auspices of the European Task Force in Age-Related White Matter Changes (ARWMC) was used to test the reliability of Lesion Explorer against an established rating scale (Pantoni et al., 2002; Wahlund et al., 2001) (reported $\kappa = 0.67$; group $\kappa = 0.89$). In brief, the severity of SH was rated on PD and T2-weighted MR images in five regions in each hemisphere: frontal, parieto-occipital, temporal, basal ganglia and infratentorial. SH were accepted if they appeared on both PD and T2 images and if they were at least 5 mm in diameter. Severity was graded from 0 (none) to 3 (severe) based on the appearance of the SH. A measure of global severity was derived by summing the ratings for the 5 regions.

MRI processing

An overview of the image processing steps is summarized in Fig. 1. Note that LE is an individualized procedure where each individual's set of scans is processed singularly and thus group analysis is not a requirement for this processing pipeline. A trained operator can process one brain in approximately 1–1.5 h/brain, depending on scan quality (motion artifacts, image contrast, etc.). The overall MRI processing pipeline has 3 main components: Brain-Sizer, SABRE, and Lesion Explorer.

Component 1 — Brain-Sizer

Brain extraction and tissue segmentation were accomplished using an updated head-from-brain (HfB) procedure from previously described methods (Kovacevic et al., 2002; Levy-Cooperman et al., 2008). In brief, the PD and T2 images were coregistered to the T1 using a rigid body transformation. In early efforts, the transformation was obtained using the Automated Image Registration v.5.2 (AIR5) and a ratio image cost function (Woods et al., 1998). However, this was found to result in misalignment for some subjects, and therefore FSL's flirt tool and a normalized mutual information cost function is now used for all coregistration (Woolrich et al., 2009). The three coregistered images were used to extract brain and sub-dural CSF from the supratentorial cranial compartment with some manual editing to create a binary mask which was applied to the 3 coregistered images (Figs. 1b–c). Automation of this process was accomplished using a template-guided procedure, using an in-house template that was generated by averaging 50 previously extracted brain scans using our previous method. The T1-template was coregistered to each subject's T1 image and the inverse transformation matrix was used to move the binary template HfB mask into subject space using nearest neighbor interpolation. The spatially transformed template HfB binary mask in subject space was then smoothed using a 3D recursive Gaussian image filter (sigma = 2). The PD-T2 images were intensity normalized to have values between 0 and 1. Voxels greater than 0.9995 on the transformed, smoothed template HfB binary mask and voxels greater than a predefined threshold value on the intensity normalized T2 (threshold = 0.35) and PD (threshold = 0.37) were accepted as brain, creating each subjects' first pass HfB binary mask. Each subjects' first pass HfB mask was smoothed using a 3D recursive Gaussian image filter (sigma = 2) and voxels greater than 0.5 were accepted as brain to create the subject's final HfB mask.

The final brain-extraction mask is manually checked and corrected for common brain-extraction errors, such as around the optic tracts and the more superior axial slices, using in-house image editing software and/or the itk-SNAP software package (Yushkevich et al., 2006). The manual checking step took approx. 1–10 min of user intervention.

Brain-Sizer's extraction procedure was developed to address the tendency for other brain-extraction methods to remove a significant number of sCSF voxels near the brain perimeter. Most brain-extraction methods (e.g., FSL's Bet, Freesurfer's MRI Watershed) operate on only the T1 image, where there is little intensity differentiation between background and sCSF (see Fig. 2). Therefore, we developed an extraction method that operates on the PD-T2 images, where there is good differentiation between all 3 types of brain voxels (GM/WM/CSF) and background. Thus, Brain-Sizer's method provides a more accurate brain-extraction mask that includes all brain and sub-dural CSF voxels.

The brain-extraction mask was applied to the T1 and automatically segmented using a previously published, in-house T1-based tissue segmentation procedure (Kovacevic et al., 2002). In brief, scanner inhomogeneity corrected segmentation was accomplished by fitting four Gaussian curves to local intensity histograms to derive intensity cut-offs for classifying voxels as WM, GM, or CSF.

Designation of ventricles and cerebellum removal was manually performed on the T1-segmentation image (T1seg), using in-house image editing software and/or a modified version of the itk-SNAP software package (Yushkevich et al., 2006). The modified itk-SNAP interface is shown in Fig. 3. The re-labeling of CSF to vCSF was accomplished by seeding and floodfilling CSF voxels on the T1seg with the T1 image for reference. This step was performed manually in order to accurately segment periventricular subcortical hyperintensities — where lesion voxels adjacent to the ventricles can often segment as CSF in fully automated procedures.

The manual steps for editing the T1seg for vCSF assignment and cerebellum removal took approx. 30–45 min of user intervention, with each brain voxel classified into one of 4 categories: WM, GM, vCSF and sCSF.

Component 2 — Semi-Automated Brain Region Extraction (SABRE)

Brain region parcellation was accomplished using an updated version of previously described methods (Dade et al., 2004). SABRE is

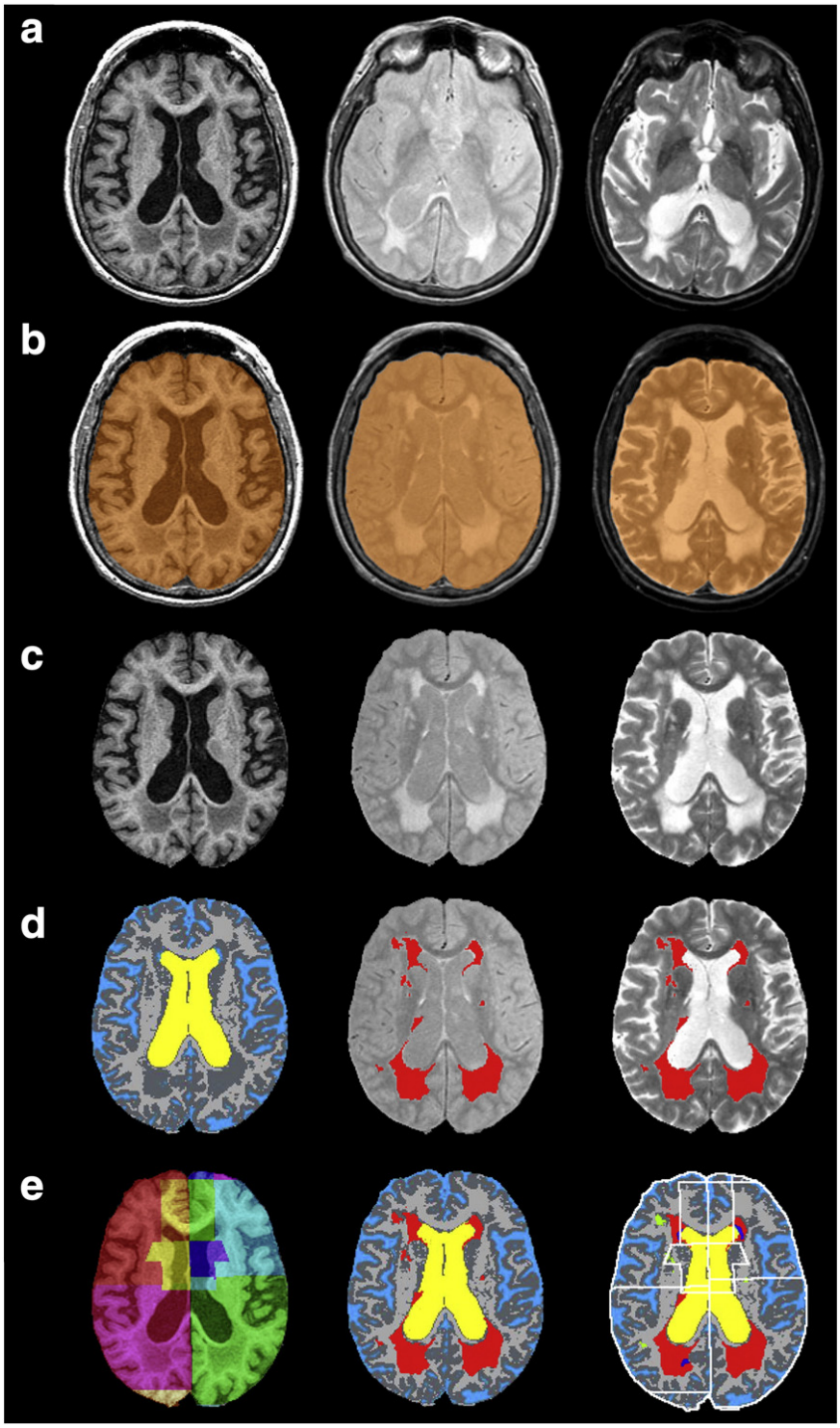

Fig. 1. Image processing steps (left to right): a) T1, PD and T2; b) PD and T2 are coregistered to T1-acquisition space and a binary mask (orange) is overlayed for brain extraction; c) brain and sub-dural CSF is extracted in preparation for tissue segmentation; d) T1-segmentation (T1seg: blue = CSF, light gray = WM, dark gray = GM), Lesion Explorer segmentation (LabVol) in red overlayed on PD-T2; e) SABRE parcellations (colors represent different SABRE regions), T1seg corrected for SH (i.e., T1seg + LabVol), corrected segmentation volumes separated into SABRE regional compartments (i.e., T1seg + LabVol + SABRE).

a quick and reliable method that was used to extract 26 brain regions proportional to individual head sizes (ICC range: 0.97–0.99 for individual tissue classes in each region). Previous studies have applied the SABRE method in studies examining multiple sclerosis (MS) and frontotemporal dementia (FTD), showing its ability to discriminate varying pathologies (Carone et al., 2006; Chow et al., 2007, 2008a,b). In brief, a set of easily identified landmarks were traced on the masked T1 images using the 3D volume render and 2D region of interest (ROI) module in ANALYZE (Biomedical Imaging Resource, Mayo Foundation, Rochester, MN, USA): the central sulcus, sylvian fissure and parieto-occipital sulcus. These tracings were combined with 7 landmarks identified in 2D on the T1 image to generate a Talairach proportional grid system which was used to create individualized maps of 13 lobular regions in each hemisphere — resulting in a total of 26 brain regions (Fig. 1e). The manual steps for SABRE landmark identification took approx. 20 min of user intervention. An updated version of SABRE uses an in-house modified version of itk-SNAP for landmark identification and reduces manual intervention by 5–10 min (Yushkevich et al., 2006).

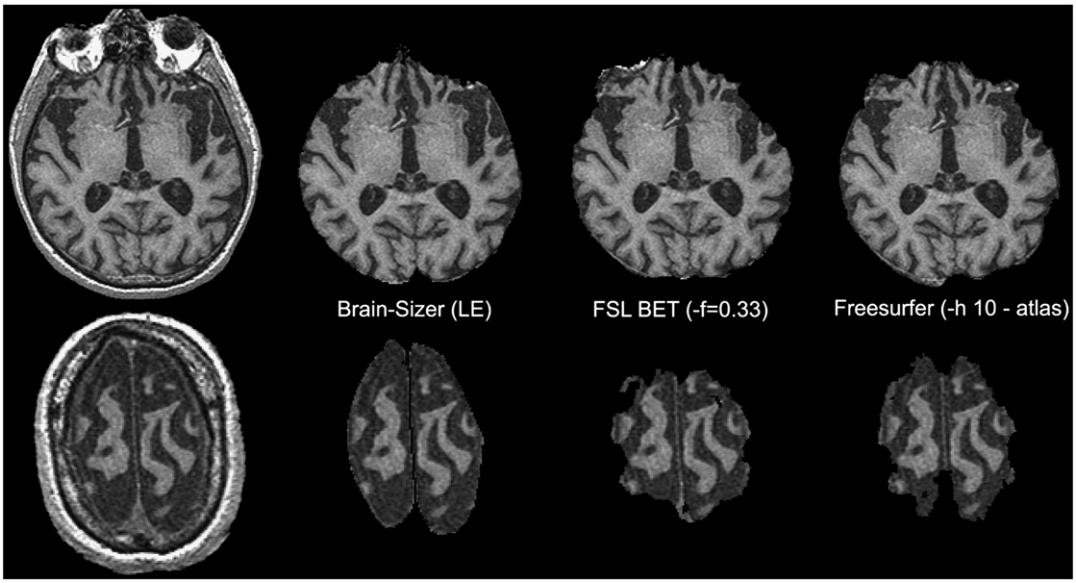

Fig. 2. A comparison of skull stripped T1 images using LE's Brain-Sizer, FSL's Brain Extraction Tool (BET) and Freesurfer using standard parameters. Accurate estimates of TIC are required to correct for individual variability in head size differences, which are particularly relevant when accounting for sex differences (Decarli et al., 2005b).

The modified itk-SNAP interface is shown in Fig. 4. Additional study-specific SABRE regions are available upon request which include: additional temporal lobe parcellations; cholinergic pathways; cingulate; thalamus.

Component 3 — Lesion Explorer: subcortical hyperintensity segmentation

Given that prior to this component, all brain voxels have been classified as GM/WM/vCSF/sCSF, the LE segmentation can be considered as a correction of the original T1seg — where previously classified voxels were reclassified as SH using additional information from the PD-T2 images. Further segmentation into pvSH, dwSH, lacunar and non-lacunar was accomplished using automated procedures.

SH segmentation was accomplished by applying an adaptive local thresholding model that was used for SH segmentation, similar to Kovacevic et al. (2002) method for dealing with inhomogeneities. The edited T1seg (obtained from the Brain-Sizer component) was first used to mask the coregistered PD and T2 for head-from-brain and vCSF removal. The brain images were subdivided into small 3D local regions to calculate thresholds, based on intensity histograms derived from the PD and T2 images. Mean and local maxima were used in this model to estimate intensity cut-offs (T) for SH as follows:

$$T = mean + P(\max - mean)$$

Where P = fractional threshold (0–1), allowing the user to calibrate the model for application to different pathologies, including

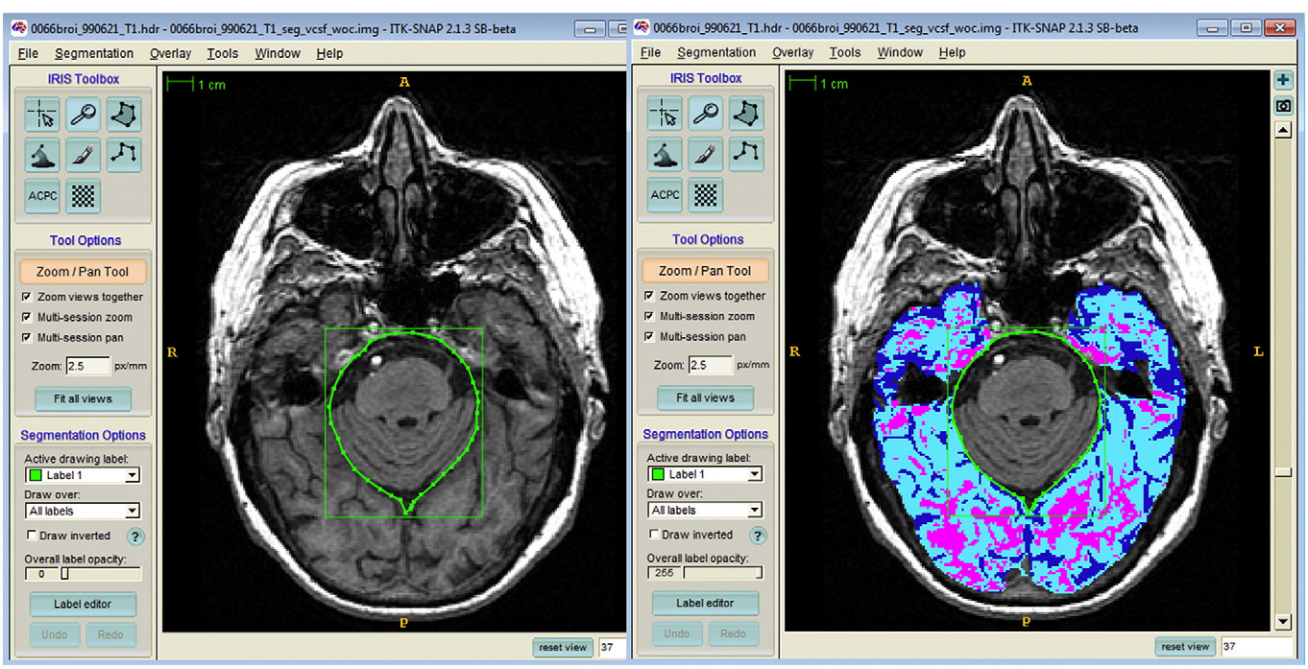

Fig. 3. In-house modified version of the itk-SNAP software package (Yushkevich et al., 2006) showing manual removal of cerebellum. The T1 is used as the reference (left) and then used to remove the sub-tentorial brain matter from the T1seg (right).

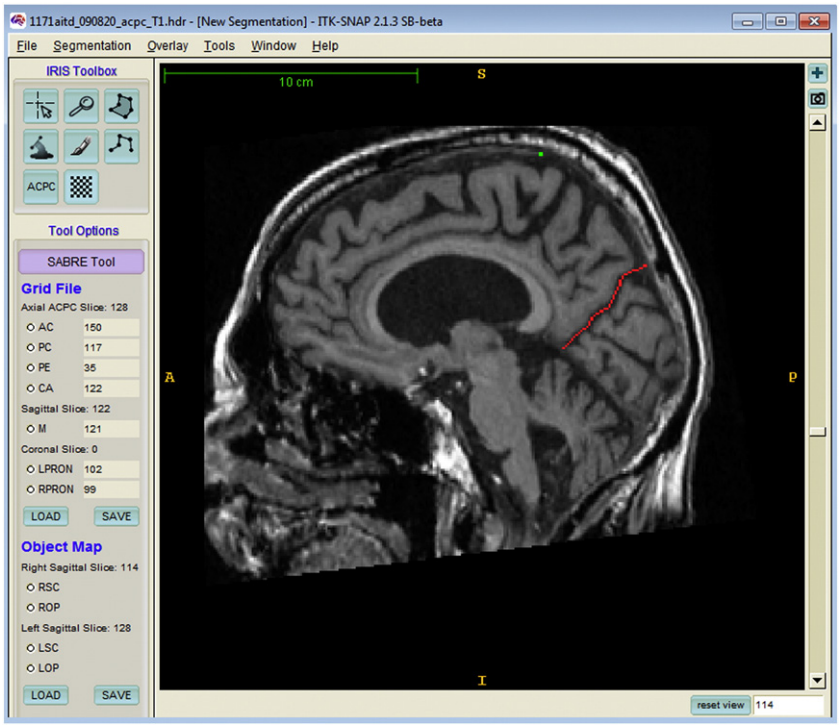

Fig. 4. In-house modified version of the itk-SNAP software package (Yushkevich et al., 2006) showing the Semi-Automated Brain Extraction (SABRE) landmark identification procedure (Dade et al., 2004). The SABRE tool-kit has grid coordinates for specified landmarks shown on the left interface panel (e.g., anterior and posterior commissure: AC–PC) and allows for the manual identification of additional structures required for SABRE regional parcellation such as the parieto-occipital sulcus traced in red (right).

cerebrovascular, and varying MRI acquisition systems. The fractional threshold was set at 0.05 for both PD and T2 on the set of reliability scans used in this study. The two SH segmentations from the PD and T2 were combined using an AND operation. The output of this step is a single labeled volume containing the segmented SH (LabVol). This automated SH segmentation method provides a simple, fast, and effective segmentation providing satisfactory initial results for further processing.

Following the initial SH segmentation, many sCSF, vCSF, and choroid plexus (CP) voxels were classified as SH. These false positive classifications were minimized using the following two-stage false positive minimization procedure.

A vCSF-CP mask was generated from the edited T1seg and subjected to the following morphological operations: a 2D dilation operation (radius = 1, cross structuring element), followed by a 2D closing operation (radius = 1, ball structuring element). Any remaining "holes" in the vCSF-CP mask were filled (where holes were defined in 2D as any region that was unreachable after flood filling from the far edge of the image). The morphological dilation and closing operations ensured that partial volume voxels near the edge of the ventricles and choroid plexus voxels were included in the vCSF-CP mask (and later removed from the SH segmentation).

A sCSF-GM mask was generated using an approach based on the fuzzy C-Means (FCM) clustering algorithm (Bezdek et al., 1997). In brief, the FCM algorithm is an unsupervised clustering technique that is used to partition datasets into "C" different classes. Each data point is assigned a "fuzzy" membership grade that represents the degree to which a data point belongs to each of the classes. To generate the sCSF-GM mask, the FCM algorithm was applied to the T1 image using 4 classes: background, CSF, GM and WM. The FCM results for the CSF class were thresholded, creating a CSF mask (threshold = 0.150) and any vCSF voxels (from the mask described above) were removed, creating a sCSF mask. Any voxels not connected in 3D to the largest object in the sCSF mask were also removed, as these voxels could be cystic lesion voxels that should be included in the SH segmentation and therefore excluded from the sCSF-GM mask. The GM compartment was then estimated by taking advantage of the fact that GM voxels are typically situated within a narrow region adjacent to sCSF voxels. Specifically, the sCSF-GM mask was generated by performing a 3D dilation operation (radius = 1, ball structuring element) on the sCSF mask, followed by the application of a 2D median filter (radius = 1), and finalized with a 2D dilation operation (radius = 1, cross structuring element).

Any voxel on the SH segmentation that corresponded to a vCSF-CP or sCSF-GM voxel on the mask images was reclassified as non-SH, thereby minimizing the number of false positive classifications. Finally, hyperintensities which were 3 voxels or less in size (in 3D) were removed from the segmentation to account for small artifacts and the exclusion of most Virchow–Robin spaces. Larger VR spaces typically found in the inferior region of the basal ganglia and thalamus were manually excluded if necessary. Virchow–Robin spaces were also defined by their relative intensity differences on PD and T2 images, where they appear hyperintense on T2, isointense on PD and hypointense (dark, CSF intensity) on T1 (see Fig. 5).

A manual checking procedure was performed by a trained operator to remove any further false positives using an in-house editing software and/or a modified version of the itk-SNAP software package (Yushkevich et al., 2006). The manual steps for checking the SH segmentation took approx 10–20 min of user intervention.

Periventricular and deep white segmentation

An automated 3D connectivity operation (3D face connectivity, 6 connected neighborhood) was applied to the edited SH segmentation (LabVol) to further segment pvSH from dwSH. Using the T1seg, all SH voxel clusters that were connected in 3D to the ventricles were subclassified as pvSH and the remaining SH voxels were classified as dwSH. In this manner, all contiguous SH adjacent to the ventricles

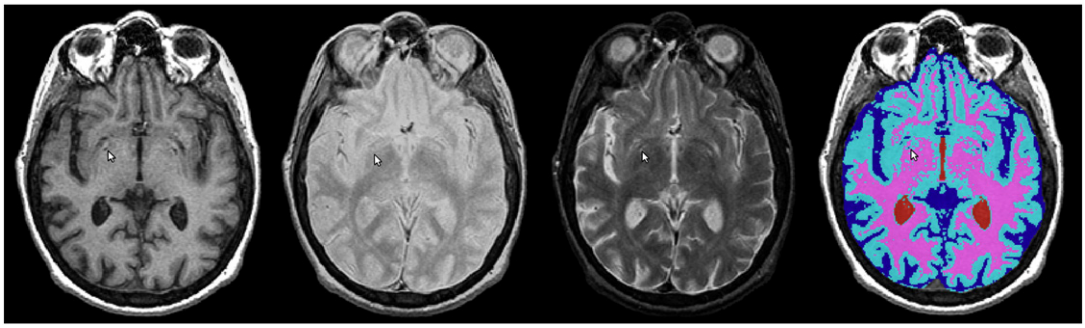

Fig. 5. (Left to right) T1, PD, T2, T1seg overlayed onto T1 (pink = WM, turquoise = GM, blue = CSF, red = vCSF). VR perivascular spaces are typically found in the inferior region of the basal ganglia and were defined by their relative intensity differences on T1, PD, and T2. From left to right, on T1 they appear hypointense (dark), on PD they appear isointense and are relatively unambiguous, on T2 they appear hyperintense, and generally segment as CSF (blue). There are several VR spaces that can be seen on both left and right basal ganglia. VR can thus be discriminated from lacunes, which generally appear hyperintense on both PD and T2 (see Fig. 7).

became classified as pvSH, and all discrete SH not connected to the ventricles became classified as dwSH (see Fig. 6).

Lacunar and non-lacunar

An automated operation was used to further segment SH into lacunar and non-lacunar subtypes. Using the T1seg, all SH voxels that segmented as CSF on the T1seg were identified as cystic fluid-filled lacunar-type infarcts within SH (see Fig. 7). The remaining voxels became classified as non-lacunar.

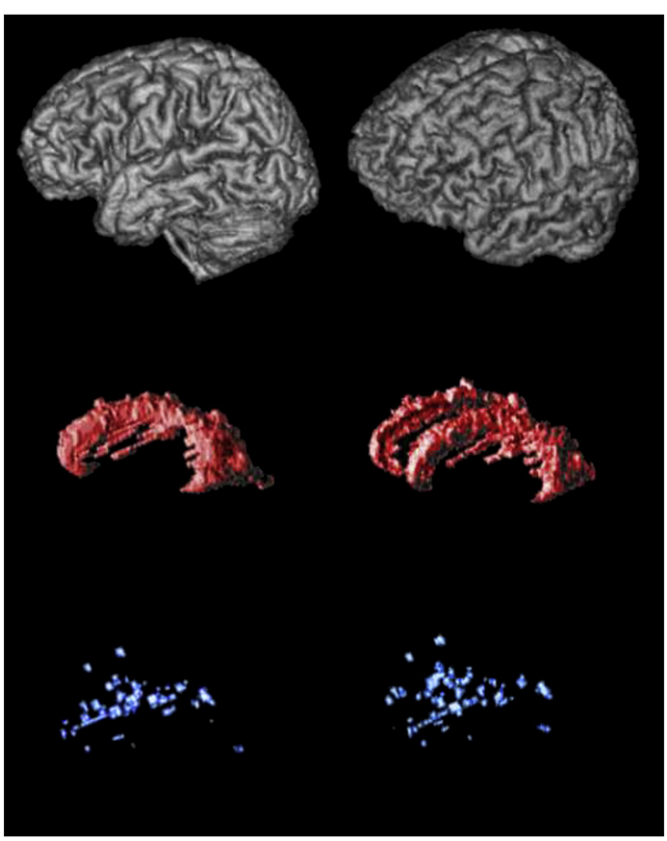

Fig. 6. 3D volume render of pvSH (red) and dwSH (blue) displayed in sagittal (left) and slightly rotated (right) 3D space. Note the red pvSH clearly appears as a single large mass surrounding the ventricles while the blue dwSH appear as several discrete masses.

Final output

The final output is a comprehensive volumetric profile of an individual's brain tissue volumes with regionalized segmentation data for: GM, WM, vCSF, sCSF, lacunar and non-lacunar pvSH, lacunar and non-lacunar dwSH in each of the 26 SABRE regions. As a final note, Brain-Sizer and Lesion Explorer components were implemented using C++ and ITK (Yoo et al., 2002).

Statistics

The volumetric data was organized into: i) whole brain and, ii) SABRE brain regions (26 volumes of interest), for statistical analysis.

Whole brain volume inter-rater reliability was determined using two trained raters who independently checked LE segmentations from 20 AD participants with varying degrees of SH. Inter-rater statistics were generated using the intra-class correlation coefficient of reliability (ICC) (Shrout and Fleiss, 2008). The mean absolute volume difference was also calculated for descriptive purposes. In addition, a kappa statistic-derived reliability measure, the Similarity Index (SI), was calculated to assess the spatial agreement of LE volumes generated by each rater as follows:

$$SI = \frac{2^{*}(Rater1 \cap Rater2)}{Rater1 + Rater2}$$

Where Rater1 ∩ Rater2 refers to the pixel-wise overlap between the two raters. The SI ranges in values from 0 to 1: where 0 indicates no spatial overlap (poor reliability) and 1 indicates perfect spatial alignment (high reliability).

Whole brain inter-method reliability was determined by comparing LE volumetrics with volumetrics generated using a previously described semi-automated segmentation based on the kNN algorithmic approach (Swartz et al., 2002; Swartz et al., 2008), and qualitative scores generated using the ARWMC scale (Wahlund et al., 2001), a consensus-derived, reliable rating scale of subcortical hyperintensities. The ICC was used with the kNN method comparison and Spearman rank correlation coefficients were used with the ARWMC score comparison.

SABRE brain region inter-rater reliability was assessed for 26 brain regions using the data from the whole brain analysis. ICC was calculated for each SABRE brain region across the 20 participants. Spearman correlation coefficients were used to compare volumes from an additional SABRE mask encompassing the lateral cholinergic

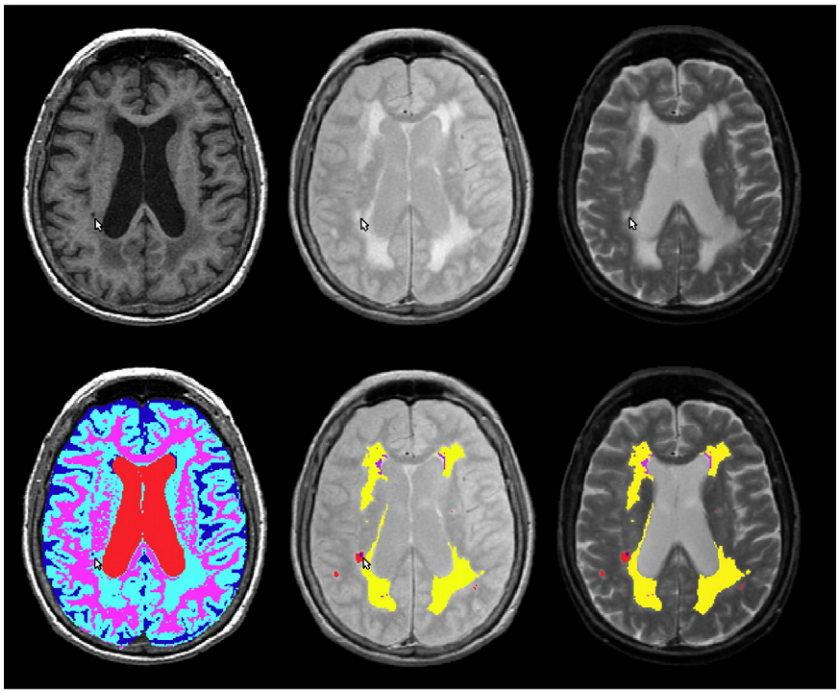

Fig. 7. Cystic fluid-filled lacunar-type infarcts such as the one shown with the arrow appear hypointense on T1 (top left), and hyperintense on both PD (top middle) and T2 (top right). The LE pipeline component automatically segments any CSF-intensity voxels (blue voxels, bottom left) within hyperintensities (bottom middle, bottom right). An additional segmentation is performed that sub-classifies them as lacunar in both deep white (blue within red) and periventricular (purple within yellow) lesion volumes. Note that the initial T1seg (bottom left) misclassifies some areas of WM (pink) as GM (turquoise) due to their darker intensity on T1 (top left), stressing the importance of an additional lesion segmentation to correct for this error in severe cases (Levy-Cooperman et al., 2008).

pathways with qualitative scores generated by a fifth rater using the Cholinergic HyperIntensities Scale (CHIPS) (Bocti et al., 2005).

Results

Whole brain results

Whole brain mean absolute volume differences between the two raters was 230 mm^3 with the following results: ICC = .99, p < .0001, and mean SI = .97, indicating excellent inter-rater reliability for whole brain volumetric and pixel-wise spatial agreement (see Table 1 for raw data). Compared to volumes from a previously published semi-automated segmentation using a kNN algorithm, high reliability was also demonstrated (ICC = .97, p < .0001). Whole brain segmentation of pvSH volumes also yielded high reliability results (ICC = .99, p < .0001). Since the pvSH segmentation showed high reliability and the pixel-wise spatial agreement as indicated by whole brain SI was also high, the remaining dwSH required no analysis. In addition, the automated lacunar segmentation also required no analysis as their volumes yield the exact same results from both raters. When compared to independently rated scores using the ARWMC, a significant high Spearman correlation was revealed (r = .86, p < .0001). See Table 2 for summary.

Regional results

Mean absolute volume difference between the two raters across all SABRE regions was 13.83 mm^3 with mean ICC = .98 [range = 0.91–0.99], indicating high regional inter-rater reliability. SABRE region ICC results are summarized in Table 2. When compared to independently rated scores using the CHIPS scale, volumes from SABRE's additional standardized cholinergic fiber region revealed a significant high Spearman correlation (r = .87, p < .0001) (Tables 3 and 4).

Discussion

Lesion Explorer is the final component of a comprehensive segmentation and parcellation package that provides an individualized volumetric profile from standard structural MRI. The overall MRI volumetrics package is a reliable application that may be used with confidence in aging populations for both cross-sectional, and longitudinal studies with a standard structural acquisition protocol.

The brain-extraction component, Brain-Sizer, provides an accurate measure of an individual's total intracranial capacity. An accurate intracranial volume is a significant and important measure as it is used for head size correction. Statistically significant differences may become not significant after correcting for head size. The large Framingham Heart Study, demonstrated this phenomenon, where men had significantly greater brain volumes as compared to women, but these differences were generally not significant after head size correction (Decarli et al., 2005b). In the Framingham study, total cranial volume was obtained

Table 2
Reliability test summary.

Reliability test	Result	p-value
Whole brain		
Mean absolute volume difference	230 mm^3	
Whole brain volumetrics	ICC = .99	p < .0001
Pixel-wise spatial agreement	SI = .97	
Periventricular SH volumes	ICC = .99	p < .0001
Inter-method (kNN segmentation)	ICC = .97	p < .0001
Inter-method (ARWMC rating scale)	r = .86	p < .0001
Regional		
Mean SABRE regions	ICC = .98	p < .01
Inter-method (CHIPS rating scale)	r = .87	p < .0001

Summary of whole brain and regional reliability tests performed by different raters on 20 AD participants with varying degrees of SH burden.

Table 3
Regional inter-class correlation coefficients (ICC).

SABRE region	ICC
LSUPF	0.99
LIF	0.99
LOBF	0.99
LMOBF	0.92
LSP	0.99
LIP	0.99
LO	0.99
LAT	0.99
LPT	0.99
LABGT	0.98
LPBGT	0.93
LMSF	0.99
LMIF	0.99
RSUPF	0.99
RIF	0.99
ROBF	0.99
RMOBF	0.91
RSP	0.99
RIP	0.99
ROBF	0.99
RAT	0.99
RPT	0.99
RABGT	0.97
RPBGT	0.99
RMSF	0.99
RMIF	0.99
Mean	0.98

ICC in 26 SABRE brain regions from 2 independent raters. Results are based on 20 participants with AD. All ICC's reported met minimum, $p<.01$ significance.

with operator guided manual tracing along the dura mater. The goal of Brain-Sizer was to obtain a similar brain-extraction output that included all sub-dural tissue (including sub-dural CSF), while minimizing exhaustive manual tracing along the dura mater. This could only be accomplished with the introduction of PD-T2, allowing for a greater contrast difference between sub-dural CSF and background voxels. All intensity-based T1 skull-stripping algorithms show the same kind of segmentation errors simply because there is little contrast between CSF and background. For certain studies and for certain patient groups with specific questions, the accuracy of most T1-based skull-stripping approaches (e.g. SPM, BET, Freesurfer) may be sufficient. However, in clinical dementia populations, such as patients with typical and atypical AD, frontotemporal degeneration and mixed dementias, focal atrophy is not uncommon, and thus, the increased accuracy of our method becomes particularly important. It is also interesting to note that despite this significant finding in the Framingham study, researchers continue to opt for quick T1-based automatic brain-extraction procedures that have a tendency to erroneously label sulcal-CSF voxels along the perimeter of the brain as background voxels (see Fig. 3).

The benefits of having tri-feature information from PD-T2 and T1 images were not limited to an accurate intracranial capacity measure. Although false positive minimization is accomplished with various masking procedures that are PD-T2-based, this process was actually dependent on proper segmentation of the ventricles from prior steps in the process that required a T1 image. Additionally, the SABRE parcellation procedure is accomplished with a T1 image, which allows for individualized regional classification of lesion volumes. Another benefit to Lesion Explorer's tri-feature segmentation is the ability to further segment subcortical hyperintensities that contain cystic fluid-filled lacunar-like infarcts in both periventricular and deep white segmentations (see Fig. 7). This specificity cannot be accomplished with PD-T2 and/or FLAIR alone. Thus, Lesion Explorer should not be understood as an isolated PD-T2-based SH segmentation. It is a comprehensive volumetric segmentation and parcellation package which utilizes information from 3 common structural MRI. Given that Lesion Explorer was built upon two previously published segmentation

Table 4
Example of the volumetric profile obtained from pipeline.

SABRE region	GM	WM	CSF	vCSF	dwSH	dwSH-L	pvSH	pvSH-L
LSUPF	7770.5	14,995.0	6062.7	0.0	0.0	0.0	2081.8	1.8
LIF	15,849.3	24,849.0	12,816.7	1240.7	38.1	0.0	8292.5	422.7
LOBF	2369.8	7733.2	4012.9	0.0	0.0	0.0	105.5	1.8
LMOBF	2404.3	6162.8	3993.4	2.7	0.0	0.0	95.7	2.7
LSP	20,008.4	31,628.7	10,235.1	51.4	54.1	0.0	6041.4	8.9
LIP	25,435.7	30,310.9	10,348.5	14,646.7	179.0	0.0	12,868.1	180.8
LO	14,674.2	31,570.2	8312.8	1044.9	2.7	0.9	6512.0	16.8
LAT	3930.4	14,158.4	7534.7	42.5	0.0	0.0	0.0	0.0
LPT	25,941.7	49,416.2	21,673.7	12,047.4	244.6	0.0	1903.6	0.0
LABGT	2756.2	4584.5	462.6	3842.7	0.9	0.0	148.0	0.9
LPBGT	3422.6	4962.0	101.9	2962.7	19.5	0.0	0.0	0.0
LMSF	7408.9	13,856.2	3867.5	8.9	36.3	0.0	1589.9	0.0
LMIF	6855.9	11,009.6	5155.2	5948.4	23.9	0.0	865.8	29.2
RSUPF	4616.4	12,900.0	8955.4	0.0	0.0	0.0	1415.3	29.2
RIF	14,881.6	24,543.3	13,006.3	271.2	0.0	0.0	10,683.5	340.3
ROBF	2485.9	6936.5	4972.6	0.0	0.0	0.0	14.2	0.0
RMOBF	3410.2	7639.3	3636.2	0.9	14.2	0.0	214.5	15.1
RSP	17,167.2	30,720.3	11,373.9	16.0	8.9	0.0	7377.0	42.5
RIP	21,746.3	27,044.2	8349.2	11,723.9	133.8	0.0	11,907.4	70.9
RO	14,785.0	31,329.1	8023.9	901.3	0.0	0.0	6730.9	24.8
RAT	3980.9	13,304.1	7501.1	22.2	4.4	4.4	0.0	0.0
RPT	26,343.2	50,451.3	23,291.9	13,313.8	16.8	0.0	2498.3	4.4
RABGT	3906.5	6953.4	313.7	3973.9	0.0	0.0	307.5	1.8
RPBGT	3278.2	3474.9	104.6	2691.5	0.0	0.0	14.2	0.0
RMSF	6074.2	12,248.6	7659.7	0.0	7.1	0.0	1591.7	0.9
RMIF	7605.6	12,819.3	5303.2	5712.6	0.0	0.0	2454.9	242.8

Discrete lesion no.	1	2	3	4	5
Volume (mm^3)	768.36	665.56	4.43	4.43	2.66
Location (final slice)	95	91	39	48	53

An example of an individual's volumetrics profile generated using the LE pipeline. Top table shows raw segmentation volumetrics in mm^3 for SABRE parcellated brain regions. SH is separated into periventricular (pvSH) and deep white (dwSH) with lacunar segmentations (pvSH-L and dwSH-L) for each SH sub-category. The supplementary table below shows discrete lacunar counts for the same subject providing size and location information for each.

(Kovacevic et al., 2002) and parcellation procedures (Dade et al., 2004), we feel that the Lesion Explorer component is the final step in the right direction, with the increasing popularity of multi-modal simultaneous segmentation techniques (Kabir et al., 2007).

This tri-feature segmentation can be viewed as a limitation, given the minimal MR acquisition requirements (T1, T2 and PD) to obtain such a comprehensive volumetric profile. However, multi-modal acquisition parameters attest to the limited information that a single MR acquisition can provide. Without a T1, tissue segmentations for GM, WM, CSF and ventricles could not be performed accurately, and without a coregistered PD-T2, VR spaces could not be delineated from lacunes and a proper head-from-brain with sub-dural CSF measures for TIC could not be performed without a significant amount of manual intervention. Until the introduction of true simultaneous multi-modal imaging, these are the minimal MR acquisition parameters required to obtain these results accurately with this processing pipeline.

The segmentation of SH into periventricular and deep white classifications remains controversial. The approaches to delineate pvSH are highly variable, ranging from arbitrary distance measures from the ventricles to proportional distances from the ventricles to the dura mater (Decarli et al., 2005a; Mayer and Kier, 1991; Sachdev et al., 2005; Silbert et al., 2008). Lesion Explorer employs a novel approach that is less arbitrary relative to other approaches — any SH voxel clusters that were connected in 3D to the ventricles were sub-classified as pvSH. Although there is no neuroanatomical justification to favor this approach over other approaches, upon viewing the 3D volume render of pvSH and dwSH (see Fig. 4), we felt this approach yielded an acceptable segmentation of pvSH which was the least arbitrary. Future research with the underlying pathology of white matter disease may result in the re-evaluation of this and other approaches (Black et al., 2009).

In contrast to the controversial pvSH and dwSH debate, the pathological significance of the lacunar sub-classification is less ambiguous. Lacunes are believed to have a more disruptive neuropathology and are associated with hypertension and increased risk of stroke and dementia (Longstreth et al., 1998; Reed et al., 2004; Vermeer et al., 2003b, 2007). These cystic fluid-filled infarctions appear as CSF intensity on the T1 image and are thus derived from a coregistered T1 segmentation with a CSF compartment (see Fig. 7). Most automatic lesion segmentations often overlook this important sub-classification as they are solely based on FLAIR imaging segmentation approaches. Furthermore, the ability to disambiguate Virchow–Robin spaces is accomplished with the intensity difference between PD and T2 images, which also cannot be accomplished accurately with FLAIR imaging alone (see Fig. 5).

The overall manual intervention processing time ranges from 45 to 75 min, with minimal CPU runtime. In contrast, the FreeSurfer segmentation software package reports 20 h of CPU runtime (2× Intel Xeon E5420) with minimal user intervention (https://surfer.nmr.mgh.harvard.edu/fswiki/ReconAllRunTimes). However, the FreeSurfer segmentation is known to fail where white matter lesions exist, which make it less than ideal for applications on an elderly population where age-related white matter changes are common. As outlined in the release notes, the final surface may not follow GM along the perimeter of the lesion (http://surfer.nmr.mgh.harvard.edu/fswiki/ReleaseNotes). A fix for this known issue may be included in a future release.

As the general progression of imaging analysis has tended towards more quick and automatic approaches, it is clear that the main bottlenecks of the Lesion Explorer processing pipeline can be found where user intervention is required (ranging from 1 to 1.5 h/brain). Despite this time constraining caveat, the individualized approach and comprehensive volumetric profile that is provided with our pipeline could not be accomplished without these manual interventions. Group-based and template-based analyses are often difficult given the large individual variability with respect to whole brain atrophy and ventricular size that is found in aging and dementia populations, especially with focal atrophy syndromes and cerebrovascular lesions which are highly variable. In this regard, the bias in our processing pipeline is evident as it was developed in conjunction with a dementia and aging clinic — where individual characterization remains relevant.

All thresholds except for the intensity normalized PD-T2 thresholds remain fixed. The normalized PD and T2 thresholds are fixed only for a given set of acquisition parameters. We believe that patient-group specific thresholds could be determined, for example in MS, compared to white matter disease from aging and vascular pathologies, and we intend to do this in future applications. Unfortunately, we cannot attest to the robustness of our pipeline when applied to multiple sites with varying parameters as we have not tested this on a multitude of inputs. However, we have had success with this method on both 1.5 T and 3 T scanners as well as data from several other sites with similar acquisition parameters (Chicago, Taiwan, Sherbrooke, Hong Kong, Buffalo, and UC San Francisco). With the 3 T data, our method generally requires suppression of the signal from fat, a standard option available on most MRI scanners, to make the separation of head from brain less laborious and time-consuming.

Finally, the Lesion Explorer processing pipeline can be quite useful in conjunction with other advanced imaging techniques. For example, current research is underway which utilizes the SH segmentation, WM segmentation, and SABRE parcellations, to generate diffusivity and fractional anisotropy measures for normal appearing white matter adjacent to varying degrees of white matter disease with diffusion tensor imaging (DTI). Likewise, this method can be used to evaluate cerebral blood flow by using contrast perfusion imaging or arterial spin labeling (ASL).

Acknowledgments

The authors gratefully acknowledge financial support from the following sources. The development and testing of this image analysis pipeline was supported by several grants, most notably from the Canadian Institutes of Health Research (MT#13129), the Alzheimer Society of Canada and Alzheimer Association (US), the Heart and Stroke Foundation Centre for Stroke Recovery, and the LC Campbell Foundation. JR receives salary support from the Alzheimer Society of Canada; BL from CIHR; NLC from U of T graduate awards including the KM Hunter studentship; AF and SEB from the Sunnybrook Research Institute; and SEB from the Departments of Medicine at Sunnybrook and U of T, including the Brill Chair in Neurology. JR, EG, NL, CS, FQG, and SEB also receive salary support from the HSF Centre for Stroke Recovery.

References

Admiraal-Behloul, F., van den Heuvel, D.M., Olofsen, H., van Osch, M.J., van der, G.J., van Buchem, M.A., Reiber, J.H., 2005. Fully automatic segmentation of white matter hyperintensities in MR images of the elderly. Neuroimage 28, 607–617.

American Psychiatric Association, 1994. Diagnostic and Statistical Manual of Mental Disorders, Fourth ed. American Psychiatric Association, Washington, DC.

Anbeek, P., Vincken, K.L., van Osch, M.J., Bisschops, R.H., van der, G.J., 2004. Automatic segmentation of different-sized white matter lesions by voxel probability estimation. Med. Image Anal. 8, 205–215.

Awad, I.A., Johnson, P.C., Spetzler, R.F., Hodak, J.A., 1986. Incidental subcortical lesions identified on magnetic resonance imaging in the elderly. II. Postmortem pathological correlations. Stroke 17, 1090–1097.

Babikian, V., Ropper, A.H., 1987. Binswanger's disease: a review 1. Stroke 18, 2–12.

Bastos Leite, A.J., van Straaten, E.C., Scheltens, P., Lycklama, G., Barkhof, F., 2004. Thalamic lesions in vascular dementia: low sensitivity of fluid-attenuated inversion recovery (FLAIR) imaging. Stroke 35, 415–419.

Bezdek, J.C., Hall, L.O., Clark, M.C., Goldgof, D.B., Clarke, L.P., 1997. Medical image analysis with fuzzy models. Stat. Methods Med. Res. 6, 191–214.

Black, S.E., Gao, F.Q., Bilbao, J., 2009. Understanding white matter disease: imaging–pathological correlations in vascular cognitive impairment. Stroke 40, S48–S52.

Bocti, C., Swartz, R.H., Gao, F.Q., Sahlas, D.J., Behl, P., Black, S.E., 2005. A new visual rating scale to assess strategic white matter hyperintensities within cholinergic pathways in dementia. Stroke 36, 2126–2131.

Burton, E.J., Kenny, R.A., O'Brien, J., Stephens, S., Bradbury, M., Rowan, E., Kalaria, R., Firbank, M., Wesnes, K., Ballard, C., 2004. White matter hyperintensities are

associated with impairment of memory, attention, and global cognitive performance in older stroke patients. Stroke 35, 1270–1275.
Carone, D.A., Benedict, R.H., Dwyer, M.G., Cookfair, D.L., Srinivasaraghavan, B., Tjoa, C. W., Zivadinov, R., 2006. Semi-automatic brain region extraction (SABRE) reveals superior cortical and deep gray matter atrophy in MS. Neuroimage 29, 505–514.
Chow, T.W., Takeshita, S., Honjo, K., Pataky, C.E., St Jacques, P.L., Kusano, M.L., Caldwell, C.B., Ramirez, J., Black, S., Verhoeff, N.P., 2007. Comparison of manual and semi-automated delineation of regions of interest for radioligand PET imaging analysis. BMC Nucl. Med. 7, 2.
Chow, T.W., Binns, M.A., Freedman, M., Stuss, D.T., Ramirez, J., Scott, C.J., Black, S., 2008a. Overlap in frontotemporal atrophy between normal aging and patients with frontotemporal dementias. Alzheimer Dis. Assoc. Disord. 22 (4), 327–335.
Chow, T.W., Izenberg, A., Binns, M.A., Freedman, M., Stuss, D.T., Scott, C.J., Ramirez, J., Black, S.E., 2008b. Magnetic resonance imaging in frontotemporal dementia shows subcortical atrophy. Dement. Geriatr. Cogn. Disord. 26, 79–88.
Dade, L.A., Gao, F.Q., Kovacevic, N., Roy, P., Rockel, C., O'Toole, C.M., Lobaugh, N.J., Feinstein, A., Levine, B., Black, S.E., 2004. Semiautomatic brain region extraction: a method of parcellating brain regions from structural magnetic resonance images1. Neuroimage 22, 1492–1502.
De Groot, J.C., De Leeuw, F.E., Oudkerk, M., Hofman, A., Jolles, J., Breteler, M.M., 2001. Cerebral white matter lesions and subjective cognitive dysfunction: the Rotterdam Scan Study. Neurology 56, 1539–1545.
De Leeuw, F.E., De Groot, J.C., Achten, E., Oudkerk, M., Ramos, L.M., Heijboer, R., Hofman, A., Jolles, J., van, G.J., Breteler, M.M., 2001. Prevalence of cerebral white matter lesions in elderly people: a population based magnetic resonance imaging study. The Rotterdam Scan Study. J. Neurol. Neurosurg. Psychiatry 70, 9–14.
Decarli, C., Fletcher, E., Ramey, V., Harvey, D., Jagust, W.J., 2005a. Anatomical mapping of white matter hyperintensities (WMH): exploring the relationships between periventricular WMH, deep WMH, and total WMH burden. Stroke 36, 50–55.
Decarli, C., Massaro, J., Harvey, D., Hald, J., Tullberg, M., Au, R., Beiser, A., D'Agostino, R., Wolf, P.A., 2005b. Measures of brain morphology and infarction in the Framingham Heart Study: establishing what is normal. Neurobiol. Aging 26, 491–510.
Fazekas, F., Chawluk, J.B., Alavi, A., Hurtig, H.I., Zimmerman, R.A., 1987. MR signal abnormalities at 1.5 T in Alzheimer's dementia and normal aging 6. AJR Am. J. Roentgenol. 149, 351–356.
Gao, F.Q., van Gaal, S., Levy-Cooperman, N., Ramirez, J., Scott, C.J., Bilbao, J., Black, S.E., 2008. Does variable progression of incidental white matter hyperintensities in Alzheimer's disease relate to venous insufficiency?, 4 ed. , pp. T368–T369.
Gosche, K.M., Velthuizen, R.P., Murtagh, F.R., Arrington, J.A., Gross, W.W., Mortimer, J.A., Clarke, L.P., 1999. Automated quantification of brain magnetic resonance image hyperintensities using hybrid clustering and knowledge-based methods. Int. J. Imag. Sci. Technol. 10, 287–293.
Hachinski, V., Iadecola, C., Petersen, R.C., Breteler, M.M., Nyenhuis, D.L., Black, S.E., Powers, W.J., Decarli, C., Merino, J.G., Kalaria, R.N., Vinters, H.V., Holtzman, D.M., Rosenberg, G.A., Wallin, A., Dichgans, M., Marler, J.R., Leblanc, G.G., 2006. National Institute of Neurological Disorders and Stroke–Canadian Stroke Network vascular cognitive impairment harmonization standards. Stroke 37, 2220–2241.
Jack Jr., C.R., O'Brien, P.C., Rettman, D.W., Shiung, M.M., Xu, Y., Muthupillai, R., Manduca, A., Avula, R., Erickson, B.J., 2001. FLAIR histogram segmentation for measurement of leukoaraiosis volume. J. Magn. Reson. Imaging 14, 668–676.
Jack Jr., C.R., Bernstein, M.A., Fox, N.C., Thompson, P., Alexander, G., Harvey, D., Borowski, B., Britson, P.J., Whitwell, L., Ward, C., Dale, A.M., Felmlee, J.P., Gunter, J.L., Hill, D.L., Killiany, R., Schuff, N., Fox-Bosetti, S., Lin, C., Studholme, C., DeCarli, C.S., Krueger, G., Ward, H.A., Metzger, G.J., Scott, K.T., Mallozzi, R., Blezek, D., Levy, J., Debbins, J.P., Fleisher, A.S., Albert, M., Green, R., Bartzokis, G., Glover, G., Mugler, J., Weiner, M.W., 2008. The Alzheimer's Disease Neuroimaging Initiative (ADNI): MRI methods. J. Magn. Reson. Imaging 27, 685–691.
Kabir, Y., Dojat, M., Scherrer, B., Forbes, F., Garbay, C., 2007. Multimodal MRI segmentation of ischemic stroke lesions. Conf. Proc. IEEE Eng. Med. Biol. Soc. 2007, 1595–1598.
Kertesz, A., Black, S.E., Tokar, G., Benke, T., Carr, T., Nicholson, L., 1988. Periventricular and subcortical hyperintensities on magnetic resonance imaging. 'Rims, caps, and unidentified bright objects'. Arch. Neurol. 45, 404–408.
Koga, H., Takashima, Y., Murakawa, R., Uchino, A., Yuzuriha, T., Yao, H., 2009. Cognitive consequences of multiple lacunes and leukoaraiosis as vascular cognitive impairment in community-dwelling elderly individuals. J. Stroke Cerebrovasc. Dis. 18, 32–37.
Kovacevic, N., Lobaugh, N.J., Bronskill, M.J., Levine, B., Feinstein, A., Black, S.E., 2002. A robust method for extraction and automatic segmentation of brain images. Neuroimage 17, 1087–1100.
Levy-Cooperman, N., Ramirez, J., Lobaugh, N.J., Black, S.E., 2008. Misclassified tissue volumes in Alzheimer disease patients with white matter hyperintensities: importance of lesion segmentation procedures for volumetric analysis. Stroke 39, 1134–1141.
Liao, D., Cooper, L., Cai, J., Toole, J.F., Bryan, N.R., Hutchinson, R.G., Tyroler, H.A., 1996. Presence and severity of cerebral white matter lesions and hypertension, its treatment, and its control. The ARIC Study. Atherosclerosis Risk in Communities Study. Stroke 27, 2262–2270.
Longstreth Jr., W.T., Manolio, T.A., Arnold, A., Burke, G.L., Bryan, N., Jungreis, C.A., Enright, P.L., O'Leary, D., Fried, L., 1996. Clinical correlates of white matter findings on cranial magnetic resonance imaging of 3301 elderly people. The Cardiovascular Health Study. Stroke 27, 1274–1282.
Longstreth Jr., W.T., Bernick, C., Manolio, T.A., Bryan, N., Jungreis, C.A., Price, T.R., 1998. Lacunar infarcts defined by magnetic resonance imaging of 3660 elderly people: the Cardiovascular Health Study. Arch. Neurol. 55, 1217–1225.
Longstreth Jr., W.T., Arnold, A.M., Beauchamp Jr., N.J., Manolio, T.A., Lefkowitz, D., Jungreis, C., Hirsch, C.H., O'Leary, D.H., Furberg, C.D., 2005. Incidence, manifestations, and predictors of worsening white matter on serial cranial magnetic resonance imaging in the elderly: the Cardiovascular Health Study. Stroke 36, 56–61.
Mantyla, R., Erkinjuntti, T., Salonen, O., Aronen, H.J., Peltonen, T., Pohjasvaara, T., Standertskjold-Nordenstam, C.G., 1997. Variable agreement between visual rating scales for white matter hyperintensities on MRI. Comparison of 13 rating scales in a poststroke cohort 15. Stroke 28, 1614–1623.
Mayer, P.L., Kier, E.L., 1991. The controversy of the periventricular white matter circulation: a review of the anatomic literature. AJNR Am. J. Neuroradiol. 12, 223–228.
McKhann, G., Drachman, D., Folstein, M., Katzman, R., Price, D., Stadlan, E.M., 1984. Clinical diagnosis of Alzheimer's disease: report of the NINCDS-ADRDA Work Group under the auspices of Department of Health and Human Services Task Force on Alzheimer's Disease. Neurology 34, 939–944.
Moody, D.M., Brown, W.R., Challa, V.R., Anderson, R.L., 1995. Periventricular venous collagenosis: association with leukoaraiosis. Radiology 194, 469–476.
Pantoni, L., Garcia, J.H., 1997. Pathogenesis of leukoaraiosis: a review. Stroke 28, 652–659.
Pantoni, L., Simoni, M., Pracucci, G., Schmidt, R., Barkhof, F., Inzitari, D., 2002. Visual rating scales for age-related white matter changes (leukoaraiosis): can the heterogeneity be reduced? Stroke 33, 2827–2833.
Reed, B.R., Eberling, J.L., Mungas, D., Weiner, M., Kramer, J.H., Jagust, W.J., 2004. Effects of white matter lesions and lacunes on cortical function. Arch. Neurol. 61, 1545–1550.
Sachdev, P., Wen, W., 2005. Should we distinguish between periventricular and deep white matter hyperintensities? Stroke 36, 2342–2343.
Sachdev, P.S., Wen, W., Christensen, H., Jorm, A.F., 2005. White matter hyperintensities are related to physical disability and poor motor function. J. Neurol. Neurosurg. Psychiatry 76, 362–367.
Sachdev, P., Chen, X., Wen, W., 2008. White matter hyperintensities in mid-adult life. Curr. Opin. Psychiatry 21, 268–274.
Sahlas, D.J., Bilbao, J.M., Swartz, R.H., Black, S.E., 2002. Clasmatodendrosis correlating with periventricular hyperintensity in mixed dementia. Ann. Neurol. 52, 378–381.
Scheltens, P., Barkhof, F., Leys, D., Pruvo, J.P., Nauta, J.J., Vermersch, P., Steinling, M., Valk, J., 1993. A semiquantative rating scale for the assessment of signal hyperintensities on magnetic resonance imaging. J. Neurol. Sci. 114, 7–12.
Seghier, M.L., Ramlackhansingh, A., Crinion, J., Leff, A.P., Price, C.J., 2008. Lesion identification using unified segmentation–normalisation models and fuzzy clustering. Neuroimage 41, 1253–1266.
Shrout, P.E., Fleiss, J.L., 2008. Intraclass correlations: uses in assessing rater reliability. Psychol. Bull. 86, 420–428.
Silbert, L.C., Nelson, C., Howieson, D.B., Moore, M.M., Kaye, J.A., 2008. Impact of white matter hyperintensity volume progression on rate of cognitive and motor decline. Neurology 71, 108–113.
Srikanth, V., Beare, R., Blizzard, L., Phan, T., Stapleton, J., Chen, J., Callisaya, M., Martin, K., Reutens, D., 2009. Cerebral white matter lesions, gait, and the risk of incident falls: a prospective population-based study. Stroke 40, 175–180.
Swartz, R.H., Black, S.E., Feinstein, A., Rockel, C., Sela, G., Gao, F.Q., Caldwell, C.B., Bronskill, M.J., 2002. Utility of simultaneous brain, CSF and hyperintensity quantification in dementia. Psychiatry Res. 116, 83–93.
Swartz, R.H., Stuss, D.T., Gao, F., Black, S.E., 2008. Independent cognitive effects of atrophy and diffuse subcortical and thalamico-cortical cerebrovascular disease in dementia. Stroke 39, 822–830.
van Swieten, J.C., Geyskes, G.G., Derix, M.M., Peeck, B.M., Ramos, L.M., van Latum, J.C., van, G.J., 1991. Hypertension in the elderly is associated with white matter lesions and cognitive decline. Ann. Neurol. 30, 825–830.
Vermeer, S.E., Den, H.T., Koudstaal, P.J., Oudkerk, M., Hofman, A., Breteler, M.M., 2003a. Incidence and risk factors of silent brain infarcts in the population-based Rotterdam Scan Study. Stroke 34, 392–396.
Vermeer, S.E., Hollander, M., van Dijk, E.J., Hofman, A., Koudstaal, P.J., Breteler, M.M., 2003b. Silent brain infarcts and white matter lesions increase stroke risk in the general population: the Rotterdam Scan Study. Stroke 34, 1126–1129.
Vermeer, S.E., Longstreth Jr., W.T., Koudstaal, P.J., 2007. Silent brain infarcts: a systematic review. Lancet Neurol. 6, 611–619.
Wahlund, L.O., Barkhof, F., Fazekas, F., Bronge, L., Augustin, M., Sjogren, M., Wallin, A., Ader, H., Leys, D., Pantoni, L., Pasquier, F., Erkinjuntti, T., Scheltens, P., 2001. A new rating scale for age-related white matter changes applicable to MRI and CT. Stroke 32, 1318–1322.
Wen, W., Sachdev, P.S., 2004. Extent and distribution of white matter hyperintensities in stroke patients: the Sydney Stroke Study. Stroke 35, 2813–2819.
Wen, W., Sachdev, P.S., Li, J.J., Chen, X., Anstey, K.J., 2008. White matter hyperintensities in the forties: their prevalence and topography in an epidemiological sample aged 44–48. Hum. Brain Mapp. 30 (4), 1155–1167.
Woods, R.P., Grafton, S.T., Holmes, C.J., Cherry, S.R., Mazziotta, J.C., 1998. Automated image registration: I. General methods and intrasubject, intramodality validation. J. Comput. Assist. Tomogr. 22, 139–152.
Woolrich, M.W., Jbabdi, S., Patenaude, B., Chappell, M., Makni, S., Behrens, T., Beckmann, C., Jenkinson, M., Smith, S.M., 2009. Bayesian analysis of neuroimaging data in FSL. Neuroimage 45, S173–S186.
Yoo, T.S., Ackerman, M.J., Lorensen, W.E., Schroeder, W., Chalana, V., Aylward, S., Metaxas, D., Whitaker, R., 2002. Engineering and algorithm design for an image processing Api: a technical report on ITK—the Insight Toolkit. Stud. Health Technol. Inform. 85, 586–592.
Yushkevich, P.A., Piven, J., Hazlett, H.C., Smith, R.G., Ho, S., Gee, J.C., Gerig, G., 2006. User-guided 3D active contour segmentation of anatomical structures: significantly improved efficiency and reliability. Neuroimage 31, 1116–1128.